

CONF-980234--

66

CUBE-TEXTURED NICKEL SUBSTRATES FOR HIGH-TEMPERATURE
SUPERCONDUCTORS

E.D. Specht, A. Goyal, D.F. Lee, F.A. List, D.M. Kroeger, M. Paranthaman,

R.K. Williams, and D.K. Christen

RECEIVED

MAY 06 1998

G.S.T./

Oak Ridge National Lab., Oak Ridge, Tennessee, 37831-6118

The biaxial textures created in metals by rolling and annealing make them useful substrates for the growth of long lengths of biaxially textured material. The growth of overayers such as high-temperature superconductors (HTS) require flat substrates with a single, sharp texture. A sharp cube texture is produced in high-purity Ni by rolling and annealing. We report the effect of rolling reduction and annealing conditions on the sharpness of the cube texture, the incidence of other orientations, the grain size, and the surface topography. A combination of high reduction, and high temperature annealing in a reducing atmosphere leads to >99% cube texture, with mosaic of 9.0° about the rolling direction (RD), 6.5° about the transverse direction (TD), and 5.0° about the normal direction (ND).

Introduction

[DTIC QUALITY INSPECTED 1]

Rolling and annealing of fcc metals such as Cu, Au, Al, and Ni leads to the {100}<100> or "cube" texture (the notation is defined in Fig. 1). This is a particularly useful texture for several reasons: it is a sharp texture, it develops with a large fraction of the sample close to the ideal orientation, and all grains in an ideal cube texture have a

DISTRIBUTION OF THIS DOCUMENT IS UNLIMITED

MASTER

The submitted manuscript has been authored by a contractor of the U.S. Government under contract No. DE-AC05-96OR22464. Accordingly, the U.S. Government retains a nonexclusive, royalty-free license to publish or reproduce the published form of this contribution, or allow others to do so, for U.S. Government purposes.

19980528 065

single orientation. The only other rolling textures for cubic crystal structures which share this last property are $\{100\}<011>$, $\{110\}<001>$, and $\{110\}<1\bar{1}0>$. Consider $\{221\}<221>$, for example: there are four variants: $(221)[1\bar{2}2]$, $(221)[\bar{1}2\bar{2}]$, $(221)[\bar{2}12]$, and $(221)[2\bar{1}\bar{2}]$. These variants are symmetry-related, so they will occur with equal frequency in a rolling texture. They are distinct orientations, with a 39° rotation required to bring one into alignment with another. A film grown epitaxially on such a substrate will contain numerous large-angle grain boundaries.

Cube-textured Ni has been used as a substrate for HTS. Its relatively high melting point and resistance to oxidation permit, with the use of buffer layers, [2-4] the epitaxial growth of $\text{YBa}_2\text{Cu}_3\text{O}_x$ [5, 6] and $\text{Tl}_{0.78}\text{Bi}_{0.22}\text{Sr}_{1.6}\text{Ba}_{0.4}\text{Ca}_2\text{Cu}_3\text{O}_9$ [7] films. In this report we discuss the optimization of the Ni substrate. What are the requirements for the substrate? In order for the superconducting overlayer (typically $\sim 1 \mu\text{m}$ thick) to be continuous, the substrate must be smooth. A flat substrate has the added benefit of promoting epitaxy. Because the critical current carried by grain boundaries HTS drops rapidly for misorientations of more than about 5° , [8] the cube texture must be sharp, so a highly-oriented epitaxial overlayer may be grown. Other textures are to be avoided. We have determined the optimum rolling reduction and annealing temperature for such a substrate.

Experimental

High-purity (99.99%), randomly-oriented Ni bar is successively rolled to thicknesses of 125 to 500 μm . Polished work rolls are used in order to produce a smooth Ni surface. We find this more convenient than polishing long lengths of Ni. Samples were annealed for 10 minutes in a mixture of 0.04 atm H_2 with 0.96 atm Ar. This provides a

DISCLAIMER

This report was prepared as an account of work sponsored by an agency of the United States Government. Neither the United States Government nor any agency thereof, nor any of their employees, makes any warranty, express or implied, or assumes any legal liability or responsibility for the accuracy, completeness, or usefulness of any information, apparatus, product, or process disclosed, or represents that its use would not infringe privately owned rights. Reference herein to any specific commercial product, process, or service by trade name, trademark, manufacturer, or otherwise does not necessarily constitute or imply its endorsement, recommendation, or favoring by the United States Government or any agency thereof. The views and opinions of authors expressed herein do not necessarily state or reflect those of the United States Government or any agency thereof.

convenient reducing atmosphere, but the H₂ is not critical to the development of the cube texture. Annealing 30 minutes at 1073 °C in high vacuum (base pressure of 9 x 10⁻⁹ Torr, operating pressure of 1.4 x 10⁻⁷ Torr) also produces an optimum texture, equivalent to that of a sample annealed in the H₂/Ar mixture. A thermocouple spot-welded to the sample measured the temperature.

Flatness was measured using atomic force and scanning electron microscopy (AFM and SEM). SEM was used to determine grain size.

The sharpness of the texture was measured using x-ray rocking curves and ϕ scans. A Cu x-ray source was used, with a graphite crystal selecting K_α radiation and a four-circle diffractometer orienting the sample. The distribution of tilts was measured by rocking the sample about the RD or TD while observing the out-of-plane (002) reflection (called a rocking curve or ω scan). The distributions of rotations was measured by rotating the sample about the ND while measuring the mixed (202) reflection (called an azimuthal or ϕ scan). Scan widths were determined by least-squares fitting to a Gaussian lineshape; we report the FWHM of the fitted curve. As detailed in the Appendix, the width of the (202) reflection overestimates the in-plane misalignment of the sample by a factor of 2. The volume fractions of different texture components were determined by integrating peaks on x-ray pole figures, collected in the Schultz (reflection) geometry. [9]

Results and Discussion

Texture

Ni retains its rolling texture [10] up to 200 °C [Fig. 2(a)]. For a 300 °C annealing temperature, the primary recrystallization texture [11] is observed, consisting of 94%

$\{100\}<100>$ (cube texture) and 6% $\{221\}<221>$ (twin texture) [Fig. 2(c)]. The twin texture results from 180° rotation of the cube texture about a $<111>$ axis. A mixture of rolling and primary recrystallization textures is observed at 250°C [Fig. 2(b)]. With increasing annealing temperature, the twin texture gradually disappears; for anneals at 1200°C and above, no twin texture is detected above background [Fig. 3(b)]. No secondary recrystallization was observed, even at 1375°C .

The cube texture gradually sharpens with increasing annealing temperature [Fig. 3(a)]. The rocking curve about the TD (out-of-plane alignment) sharpens from 9° to 7° FWHM. The $(202)\phi$ scan sharpens from 12° to 7° , which corresponds to an in-plane alignment sharpening from 6° to 4° (see Appendix). Because our primary concern is with rapid processing, we have not systematically investigated the effects of longer anneals. We have verified that the cube texture sharpens with increasing annealing time as well as with increasing annealing temperature. A sample annealed 10 min. at 600°C had (002) and (202) scan widths of 9.6° and 11.4° . Annealing the same sample a further 1000 min. sharpened these widths to 8.0° and 10.4° .

The $125\text{ }\mu\text{m}$ thickness used to measure the effects of different temperatures produces a sharper cube texture than thicker samples (Table I). The breadth of the cube texture increases slowly; the $(202)\phi$ scan FWHM increases 47% to 10.7° at $500\text{ }\mu\text{m}$. Sample-to-sample variability, however, increases dramatically, rising six-fold to a standard deviation of 3.1. This is undesirable, since the current carried by a long wire is determined by its weakest segment. Note that these results were obtained by varying the degree of rolling reduction; further study is needed of the effects of varying the final

sample thickness at a constant reduction by changing both the initial and the final sample thickness. Future work will also address the effects of reduction below 125 μm .

Grain growth

Between 200 and 300 $^{\circ}\text{C}$, cube textured grains nucleate with a 1 μm average grain size [Figs. 3(c) 4(a)]. Between 300 and 600 $^{\circ}\text{C}$, grain coarsening occurs until the average grain size reaches half the sample thickness [Figs. 3(c) 4(b,c)]. Secondary recrystallization is signaled by the appearance of a few very large grains. No evidence for this is seen, as the maximum grain size is always about twice the average [Fig. 3(c)]. Note that the texture continues to sharpen well beyond the temperature at which grain growth is complete [Fig. 3(a,c)], indicating that the sharpening is due to the rotation of existing grains rather than to selective grain growth.

These results are dramatically different from those of Makita *et al.* [11] Using lower-purity Ni (99.95% vs. 99.99%), they find that grain growth occurs at higher temperatures (500 to 1300 $^{\circ}\text{C}$), even with much longer annealing times (1 to 2 hours). Further, they find that secondary recrystallization occurs once the grain size reaches its final value; in our samples final grain size is reached at 600 $^{\circ}\text{C}$ but secondary recrystallization does not occur up to 1375 $^{\circ}\text{C}$.

Flatness

Average roughness of AFM line scans over a $50 \times 50 \mu\text{m}^2$ area of as-rolled Ni is 10 nm. The surface begins to roughen at 600 $^{\circ}\text{C}$, on the completion of grain growth. As described by Mullins [12], roughening is caused by grooves which develop at the grain boundaries (Fig. 5). Further study is needed to quantify this roughness.

Conclusions

A wide range of annealing temperatures (300 to 1375 °C) lead to the development of cube texture in high-purity Ni. Higher temperatures lead to a sharper texture, but produce a rougher surface. A thickness of 125 μm leads to an optimum texture.

We thank J.D. Budai for helpful discussions, and X. Cui for pointing out the variation of ϕ scan width with sample tilt. This research was sponsored by the U.S. Department of Energy, Office of Energy Efficiency and Renewable Energy, Office of Utility Technology-Superconductivity Program and Division of Materials Sciences under Contract no. DE-AC05-96OR22464 with Lockheed Martin Energy Research.

Appendix: Width of ϕ Scans

The distribution of sample tilts about the RD or TD (the out-of-plane alignment) is readily measured by a rocking curve for an out-of-plane peak (a reflection from planes parallel to the surface). Measuring the distribution of rotations about the ND (the in-plane alignment) is more difficult. A ϕ scan for an in-plane peak (a reflection from planes orthogonal to the surface) measures in-plane alignment but presents instrumental difficulties. Measurements made in transmission typically require high-energy x rays and provide low sensitivity to thin films. Measurements made in reflection require the use of small glancing angles.

In this work we follow the common practice of using ϕ scans from mixed peaks (those which are neither in-plane nor out-of-plane) as a measure of in-plane alignment. In this Appendix, we present a simple model relating ϕ scan width to in-plane alignment, and show that the width can be substantially overestimated.

Both the in-plane and out-of-plane sample alignments contribute to the width of a ϕ scan for a mixed peak. Consider a scan taken at a tilt $90-\chi$ from the ND and an azimuth ϕ from the RD, and let W_{ND} , W_{RD} , and W_{TD} be the widths of the distributions of tilts and rotations about the three principle directions. As derived by Srikant *et al.*, [13] the ϕ scan width will be the convolution of three distributions with widths:

$$\Delta\phi_{RD} = W_{RD}|\tan \chi \cos \phi|, \Delta\phi_{TD} = W_{TD}|\tan \chi \sin \phi|, \text{ and } \Delta\phi_{ND} = W_{ND}. \quad (1)$$

We have expanded Srikant *et al.*'s results to first order in the widths and converted rocking curve widths to ϕ scan widths. Assuming Gaussian distributions, the total width will be:

$$W_\phi = \sqrt{(W_{RD} \tan \chi \cos \phi)^2 + (W_{TD} \tan \chi \sin \phi)^2 + W_{ND}^2}. \quad (2)$$

For an isotropic sample, $W_{ND} = W_{RD} = W_{TD} \equiv W$, and $W_\phi = W / \cos^2 \chi$. In this case, a ϕ scan for a (202) reflection will overestimate the in-plane width by a factor of 2.

We compare the predictions of Eq. 2 with ϕ scan widths for cube-textured Ni. Rocking curves of the Ni(002) at $\phi = 0^\circ$ and 90° show that $W_{RD} = 9.1^\circ$ and $W_{TD} = 6.9^\circ$. The in-plane alignment was measured using ϕ scans of the eight {200} and {220} reflections, which are centered at $\chi = 0^\circ$. At this angle, the sample is edge-on in the beam and no diffraction is observed, so the scans were taken at $\chi = 5^\circ$, the tilt at which diffracted intensity is maximum. The mean and standard deviation for the eight scans is $W_{ND} = 5.0 \pm 0.75$. Due to the large grain size of the samples, all scans are noisy, consisting of sharp peaks from a few hundred grains. The in-plane scans were taken 5° off-center in χ , so fewer grains diffracted, and the noise-induced variation in peak width was larger.

Typical ϕ scans are shown in Fig. 6. In Table II, measured widths are compared with those calculated using Eq. 2. Good quantitative agreement is observed in all cases.

For Ni substrates and for typical buffer layers, the (111) reflection provides the best measure of in-plane mosaic W_{ND} . Accuracy can be improved by measuring W_{RD} and W_{TD} from (002) rocking curves and using Eq. (2) to deduce W_{ND} from W_ϕ . As the reader may have noticed, we reached this conclusion only after collecting the (202) ϕ scans presented here. Do as we say, not as we do! Due to their highly anisotropic growth rates, HTS films grown on smooth substrates typically have much smaller W_{RD} and W_{TD} than the substrates. As a result, $W_\phi \approx W_{ND}$, and peak selection becomes less critical.

Table I. Out-of-plane and in-plane mosaic for cube-textured Ni rolled to different thicknesses. Values are mean \pm standard deviation.

Thickness (μm)	$\Delta\omega$ Ni(002) (deg. FWHM)	$\Delta\phi$ Ni(202) (deg. FWHM)
125	6.1 ± 0.3	7.3 ± 0.5
250	6.9 ± 0.6	8.75 ± 0.8
500	7.1 ± 1.1	9.9 ± 1.9

Table II. Comparison of observed ϕ scan widths to those calculated using Eq. 2

(hkl)	χ	ϕ	W_ϕ (observed)	W_ϕ (calculated)
(113)	65°	45°	20.9	18.0°
($\bar{1}$ 13)	65°	135°	20.5	18.0°
(1 $\bar{1}$ 3)	65°	225°	21.8	18.0°
($\bar{1}$ 13)	65°	315°	21.0	18.0°
(202)	45°	0°	10.8°	10.4°
(022)	45°	90°	8.5°	8.5°
($\bar{2}$ 02)	45°	180°	10.8°	10.4°
(0 $\bar{2}$ 2)	45°	270°	8.3°	8.5°
(111)	35°	45°	7.0°	7.5°
($\bar{1}$ 11)	35°	135°	7.1°	7.5°
(1 $\bar{1}$ 1)	35°	225°	7.2°	7.5°
($\bar{1}$ 11)	35°	315°	7.6°	7.5°

Figure Captions

Fig. 1. Definition the notation for the cube rolling texture.

Fig. 2. (111) pole figures for 125 μm thick Ni. Contour intervals, selected to highlight weak texture components are: 0.1, 0.3, 1.0, 3.0, and 10.0. Annealing temperature ($^{\circ}\text{C}$): (a) 200 (b) 250 (c) 300 (d) 1372.

Fig. 3. Parameters for samples annealed 10 min. in 4% H_2 : (a) out-of-plane and in-plane alignment (b) fraction of $\{221\}<221>$ texture, and (c) mean and maximum grain size (dashed line indicates sample thickness).

Fig. 4. Grain growth, imaged by SEM.

Fig. 5. Grain boundary grooving, imaged by SEM.

Fig. 6. ϕ scans from different reflections for the same cube-textured Ni sample, with FWHM indicated.

References

1. C. S. Barrett and T. B. Massalski, *Structure of Metals* (McGraw-Hill, 1966).
2. D. K. Christen, *et al.*, Czech. J. of Physics **46**, 1531 (1996).
3. M. Paranthaman, *et al.*, Physica C **275**, 266 (1997).
4. Q. He, *et al.*, Physica C **275**, 155 (1997).
5. A. Goyal, *et al.*, Appl. Phys. Lett. **69**, 1795 (1996).
6. D. P. Norton, *et al.*, Science **274**, 755 (1996).
7. Z. F. Ren, *et al.*, J. Superconduct. (submitted).
8. D. Dimos, P. Chaudhari, J. Mannhart, and F. K. LeGoues, Phys. Rev. Lett. **61**, 219 (1988).
9. Schultz, J. Appl. Phys. **20**, 1030 (1949).
10. R. K. Ray, Acta Metall. **43**, 3861 (1995).
11. H. Makita, S. Hanada, and O. Izumi, Acta Metall. **36**, 403 (1988).
12. W. W. Mullins, J. Appl. Phys. **28**, 333 (1957).
13. V. Srikant, J. S. Speck, and D. R. Clarke, J. Appl. Phys. **82**, 4286 (1997).

Fig. 1

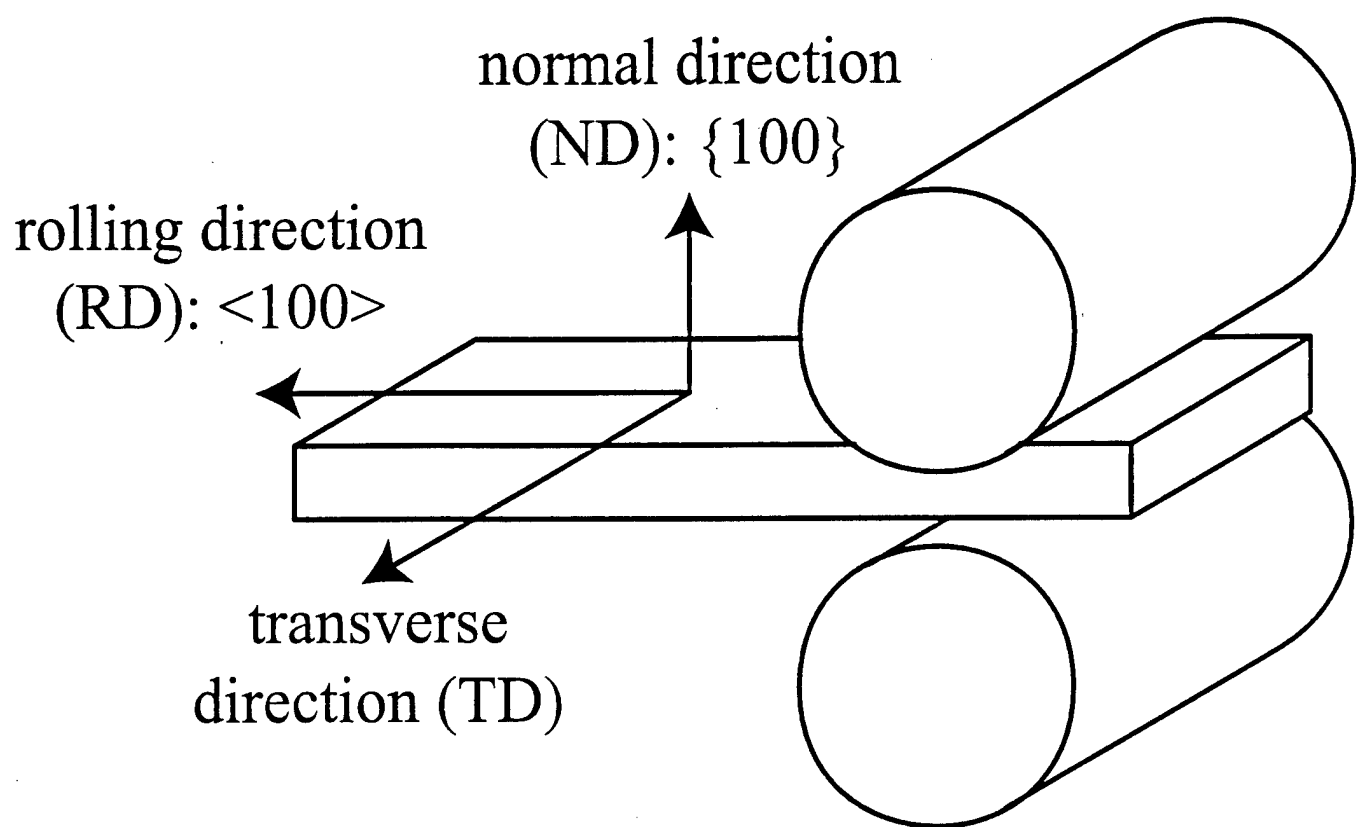


Fig. 2

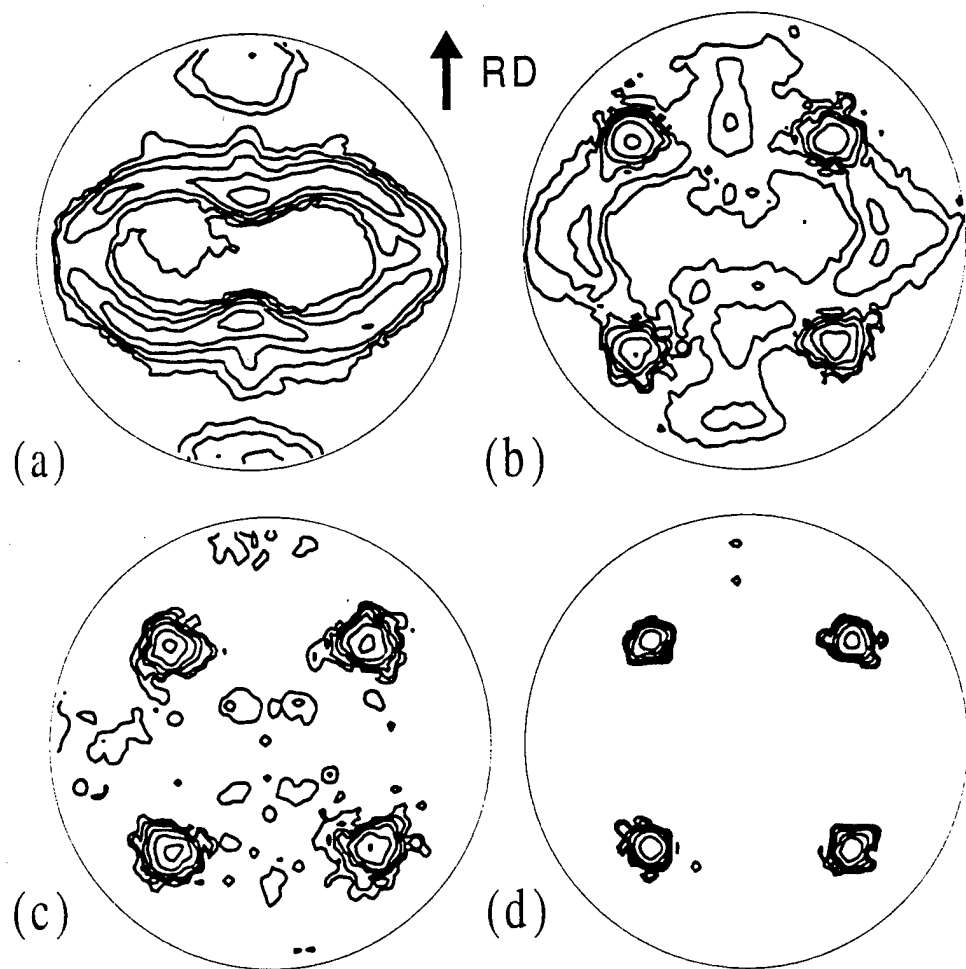


Fig. 3

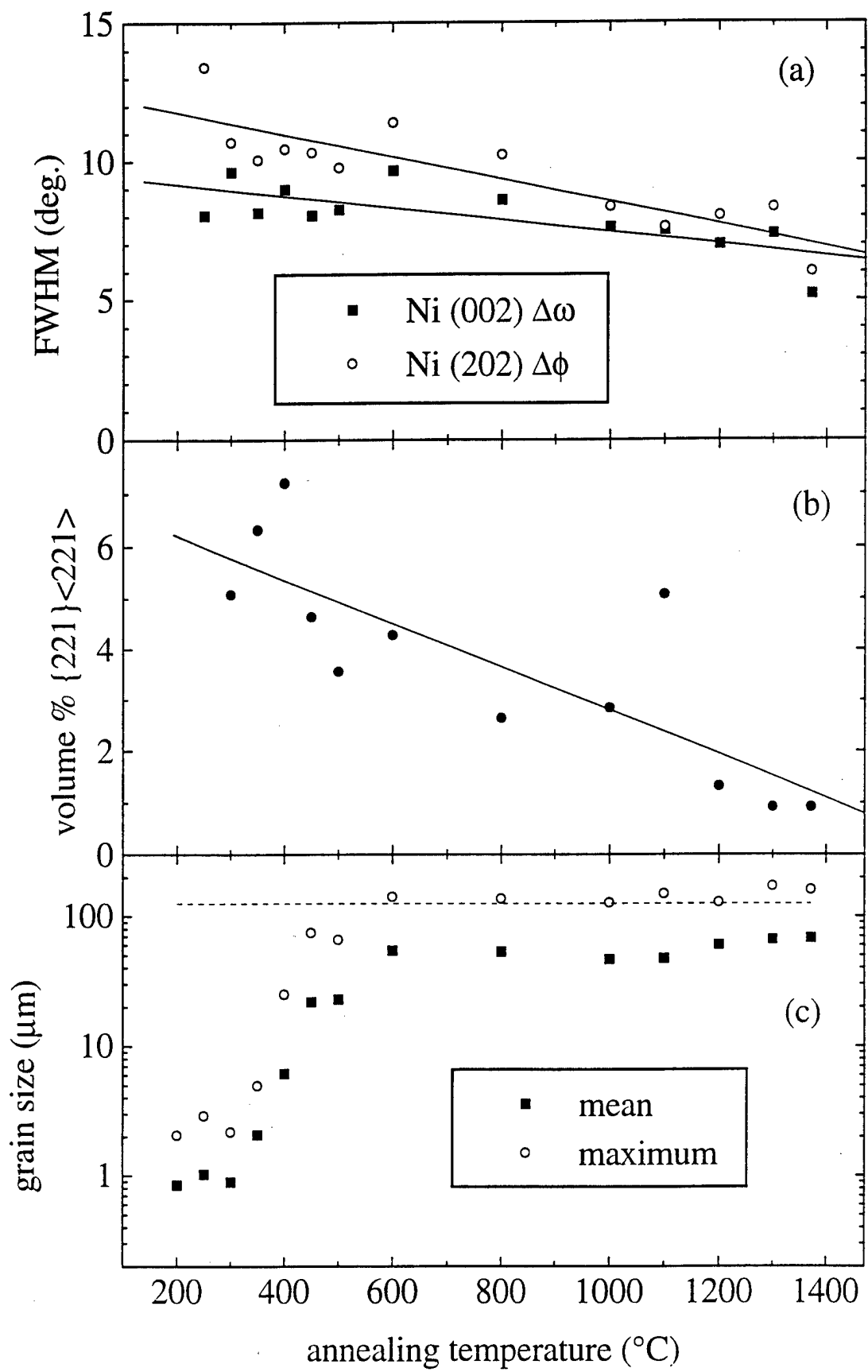


Fig. 4

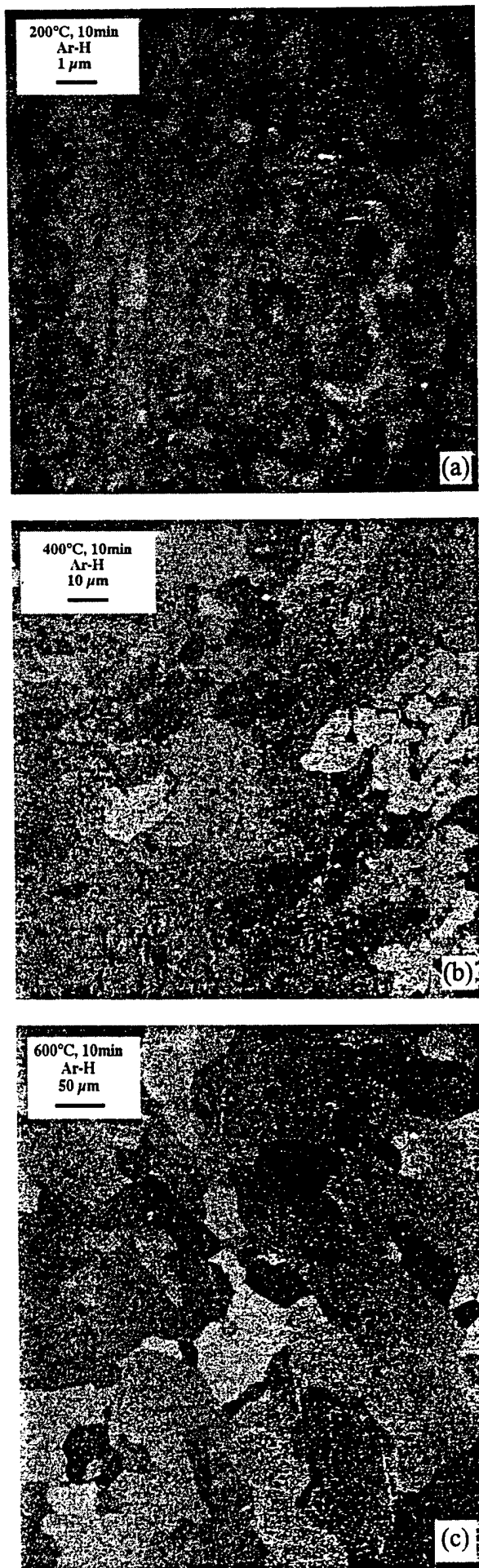


Fig. 5

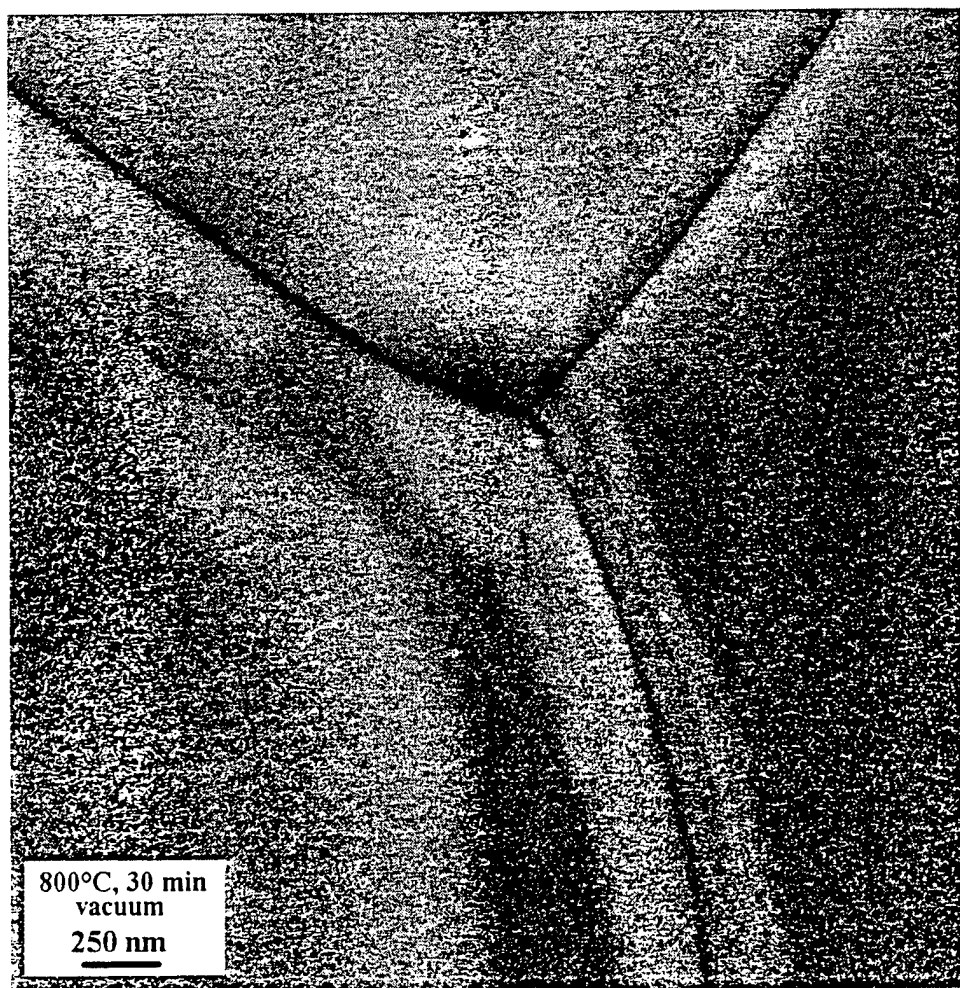
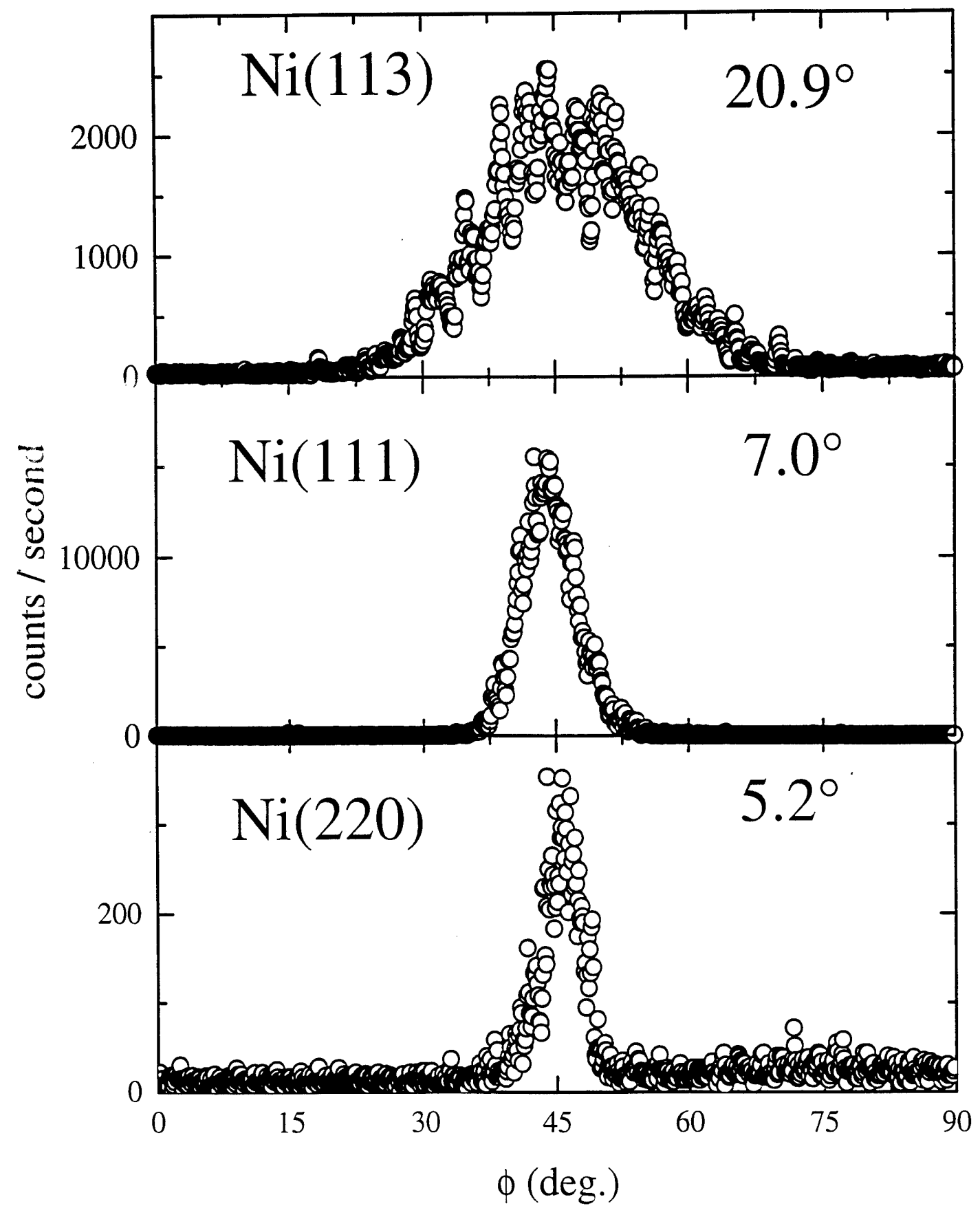


Fig. 6



M98004902



Report Number (14) ORNL/CP--97500

CONF-980234

Publ. Date (11) 199802

Sponsor Code (18) ^{DOE} ER, XF

UC Category (19) UC-404, DOE/ER

DOE